

# PROTEIN STRUCTURE REPORT

## Structure and dynamics in solution of the stop codon decoding N-terminal domain of the human polypeptide chain release factor eRF1

Vladimir I. Polshakov,<sup>1\*</sup> Boris D. Eliseev,<sup>2</sup> Berry Birdsall,<sup>3</sup>  
and Ludmila Yu. Frolova<sup>2</sup>

<sup>1</sup>Center for Magnetic Tomography and Spectroscopy, Faculty of Fundamental Medicine, M.V. Lomonosov Moscow State University, Moscow 119991, Russia

<sup>2</sup>Engelhardt Institute of Molecular Biology, Russian Academy of Sciences, 119991 Moscow, Russia

<sup>3</sup>Division of Molecular Structure, MRC National Institute for Medical Research, The Ridgeway, Mill Hill, London NW7 1AA, United Kingdom

Received 7 February 2012; Revised 15 March 2012; Accepted 17 March 2012

DOI: 10.1002/pro.2067

Published online 30 March 2012 proteinscience.org

**Abstract:** The high-resolution NMR structure of the N-domain of human eRF1, responsible for stop codon recognition, has been determined in solution. The overall fold of the protein is the same as that found in the crystal structure. However, the structures of several loops, including those participating in stop codon decoding, are different. Analysis of the NMR relaxation data reveals that most of the regions with the highest structural discrepancy between the solution and solid states undergo internal motions on the ps–ns and ms time scales. The NMR data show that the N-domain of human eRF1 exists in two conformational states. The distribution of the residues having the largest chemical shift differences between the two forms indicates that helices  $\alpha 2$  and  $\alpha 3$ , with

---

*Abbreviations:* CBCA(CO)NH, 3D experiment correlating the amide NH with the C $\alpha$  and C $\beta$  signals of the preceding amino acid; C-eRF1 or C-domain, C-terminal domain (or domain 3) of class-1 polypeptide chain release factor; eRF1, eukaryotic class-1 polypeptide chain release factor; eRF3, eukaryotic class-2 polypeptide chain release factor 3; HNCACB, 3D experiment correlating the amide NH with the C' signal of the preceding amino acid; HNCO, 3D experiment correlating the amide NH with the C' signal of the preceding amino acid; HSQC, heteronuclear single quantum coherence spectroscopy; M-eRF1 or M-domain, eRF1 middle domain (or domain 2); N-eRF1 or N-domain, N-terminal domain (or domain 1) of class-1 polypeptide chain release factor; NOE, nuclear Overhauser effect; NOESY, nuclear Overhauser enhancement spectroscopy; RDC, residual dipolar coupling;  $R_1$ , longitudinal or spin–lattice relaxation rate;  $R_2$ , transverse or spin–spin relaxation rate;  $R_{ex}$ , conformational exchange contribution to  $R_2$ ; RF, release factor; RMSD, root-mean-square deviation;  $S^2$ , order parameter reflecting the amplitude of ps–ns bond vector dynamics.

Additional Supporting Information may be found in the online version of this article.

Grant sponsor: the Russian Foundation for Basic Research; Grant numbers: 10-04-13308 (VP), 11-04-00974 (VP) and 11-04-00840 (LF); Grant sponsor: the Russian Ministry of Education and Science; Grant number: 16.740.11.0445 (VP); Grant sponsor: Presidium of Russian Academy of Sciences, the Program “Molecular and Cellular Biology” (LF).

\*Correspondence to: Vladimir I. Polshakov, Center for Magnetic Tomography and Spectroscopy, Faculty of Fundamental Medicine, M.V. Lomonosov Moscow State University, Vorobievsky Gory, GSP-1, Moscow, 119991, Russia. E-mail: vpolsha@mail.ru

the NIKS loop between them, can switch their orientation relative to the  $\beta$ -core of the protein. Such structural plasticity may be essential for stop codon recognition by human eRF1.

**Keywords:** termination of protein synthesis; human polypeptide release factor eRF1; N-domain; NMR structure and dynamics; stop codon recognition

## Introduction

The molecular mechanism of translation is the focus of intensive studies. While most aspects of this complex process have been explored in detail, the mechanism of termination still has several unanswered questions. The mechanism of stop codon recognition by the class 1 eukaryotic release factor eRF1 is one of such issues (reviewed in Refs. 1 and 2). It has been determined that the prokaryotic release factors, RF1 and RF2, recognize pairs of stop codons (UAG/UAA and UGA/UAA, respectively) through interactions with the so-called tripeptide “anticodon” regions of mRNA.<sup>3–6</sup> In contrast to their prokaryotic analogues, the eukaryotic termination factor, eRF1, from organisms using the universal genetic code is equally able to recognize all three stop codons (reviewed in Ref. 7).

The crystal structure of eRF1<sup>8,9</sup> shows that the protein contains three spatially separated domains (the N-, M-, and C- domains). Functional analysis of eRF1<sup>10</sup> has suggested that the N-terminal domain is involved in stop codon recognition. More recently, the role of the N-domain has been confirmed unambiguously: chimeric eRF1s, in which the N- and MC-domains were derived from variant-code ciliate organisms<sup>11,12</sup> and human/yeast eRF1, respectively, exhibit ciliate stop codon decoding specificity *in vitro*.<sup>13–16</sup> Several hypotheses for the molecular mechanism of stop codon recognition by eRF1 have been suggested,<sup>9,17–23</sup> but none satisfactorily explain the available experimental data which are somewhat contradictory.

High-quality structural information is essential for understanding the nature of the mRNA–eRF1 interaction. However, atomic resolution data for eukaryotic termination complexes are unavailable; and the quality of the eRF1 crystal structures<sup>8,9</sup> also leaves something to be desired, as several regions of the protein are ill-defined. Previously we determined the structure of the middle (M) and C-terminal domains of human eRF1 in solution.<sup>24,25</sup> Clear distinctions between the protein conformations in solution and in crystals were found for both the M- and the C-domains, especially for their functionally important regions. Some chemical shift assignments for a limited set of the signals (C $\alpha$ , C $\beta$ , <sup>1</sup>HN, and <sup>15</sup>N) of the N-domain of human eRF1 have been reported<sup>26</sup> but the structure of the N-domain in solution was not determined. Here we report the high-resolution solution NMR structure of the N-terminal domain of human eRF1, responsible for stop codon decoding, and present data on its dynamics.

## Results

**Resonance assignment.** <sup>1</sup>H, <sup>13</sup>C, and <sup>15</sup>N chemical shifts were assigned for ~99% of the protein backbone resonances of the isolated N-domain. More than 85% of all the side chain <sup>1</sup>H, <sup>13</sup>C, and <sup>15</sup>N chemical shifts were also assigned. The amide HN and <sup>15</sup>N signals of the residue Asn86 could not be observed in the <sup>15</sup>N–<sup>1</sup>H HSQC spectra and the signals of residues Arg65, Glu103, and Thr133 had reduced intensities, probably due to fast exchange with water. Several residues had duplicate sets of signals with a ratio of intensities of ~5:1 (Supporting Information Fig. S1). This indicates the presence of at least two conformational states of the protein.

**Structure determination.** A family of 20 NMR structures was determined on the basis of 3092 experimental restraints measured at 298 K (see Table I and Supporting Information Fig. S2). The statistics of the final ensemble are given in Table I and the superposition of the final calculated family is presented in Figure 1(A) (the backbone atoms of the N-domain of the human eRF1 crystal structure<sup>8</sup> are also shown in red for comparison). The RMSD of the calculated family from the representative structure is less than 0.5 Å for the backbone heavy atoms of the residues 6–142. In the Ramachandran plot analysis (Supporting Information Fig. S3), 93.3% of the residues in the whole NMR family were found in the most favored regions and none in the disallowed regions.

**Backbone dynamics.** Supporting Information Figure S4 presents the experimentally obtained relaxation rates  $R_1$  and  $R_2$  and NOE values for the amide <sup>15</sup>N nuclei measured at 298 K, the calculated values of the order parameter  $S^2$  and the conformational exchange contributions to the transverse relaxation rates  $R_{ex}$ . The relaxation parameters were obtained using a model with an axially symmetric diffusion tensor. The order parameter is smallest for the N- and C-terminal residues and also for the residues in several loops (30–33, 64, 106–108, 122–123). This indicates the regions in the structure where there is the highest amplitude of internal motions. The average correlation time ( $1/(2D_{\parallel} + 4D_{\perp})$ ) was  $11.04 \pm 0.16$  ns and the ratio of the principal axis of the tensor ( $D_{\parallel}/D_{\perp}$ ) was  $1.6 \pm 0.1$ . The best model that allows the most successful fit of the experimental data is that based on two internal motions with

**Table I.** NMR Restraints and Structural Statistics for the N-Terminal Domain of *Homo sapiens* Polypeptide Chain Release Factor eRF1

A. Restraints used in the structure calculation			
Total NOEs	2631	Total dihedral angles	316
Long range ( $ i - j  > 4$ )	519	Phi ( $\phi$ )	126
Medium ( $1 <  i - j  \leq 4$ )	494	Psi ( $\psi$ )	126
Sequential ( $ i - j  = 1$ )	638	Chi1 ( $\chi_1$ )	64
Intraresidue	975		
Ambiguous	5		
H-bonds	76	Residual dipolar couplings	69
B. Restraint violations and structural statistics (for 20 structures)			
No NOE or dihedral angle violations are above 0.1 Å and 2°, respectively.			
No residues are in disallowed regions of the Ramachandran plot.			
C. Superimposition on the representative structure (Å)			
CNS energies (kcal mol <sup>-1</sup> ) <sup>a</sup>	$\langle S \rangle$ <sup>b</sup>	$S_{\text{rep}}$	
$E_{\text{NOE}}$	6.46 ± 0.87	6.83	
$E_{\text{CDIH}}$	0.84 ± 0.24	1.08	
$E_{\text{SANI}}$	1.84 ± 0.14	1.54	
Average RMSD			
From experimental restraints			
Distance (Å)	0.0059 ± 0.0005	0.0060	
Dihedral (°)	0.1459 ± 0.0206	0.1680	
From idealised covalent geometry			
Bonds (Å)	0.0012 ± 0.0001	0.0013	
Angles (°)	0.3312 ± 0.0053	0.3320	
Impropers (°)	0.1915 ± 0.0118	0.1880	
% residues in the most favorable regions of Ramachandran plot	93.3	93.7	
% residues in additional allowed regions of Ramachandran plot	6.2	4.8	
C. Superimposition on the representative structure (Å)			
Backbone (C, C $\alpha$ , N) RMSD of the residues 6–142	0.510 ± 0.087		
Heavy-atom RMSD of residues 6–142	1.031 ± 0.076		

<sup>a</sup>  $E_{\text{NOE}}$ ,  $E_{\text{CDIH}}$ , and  $E_{\text{SANI}}$  are the values of NOE, dihedral angle, and residual dipolar coupling energy target functions. The final force constants used for their calculation in the simulated annealing protocol were 50 kcal mol<sup>-1</sup> Å<sup>2</sup> for NOE and 50 kcal mol<sup>-1</sup> grad<sup>2</sup> for dihedral angles.

<sup>b</sup>  $\langle S \rangle$  is the ensemble of 20 final structures;  $S_{\text{rep}}$  is the representative structure, selected from the final family on the criteria of having the lowest sum of pairwise RMSD relative to the remaining structures in the family.

correlation times of  $1.05 \pm 0.05$  ns and  $<50$  ps (Supporting Information Fig. S5).

**Comparison of the crystal and solution structures.** The topology of the N-domain of human eRF1 can be described as a  $\beta$ -sheet core formed from four anti-parallel  $\beta$ -strands, surrounded by four helices,  $\alpha_1$ – $\alpha_4$  [Fig. 1(B)]. There are also a number of loops of differing lengths, some of which are reported to be involved in stop codon recognition. For example, the loop between helices  $\alpha_2$  and  $\alpha_3$  contains conserved NIKS tetrapeptide. The overall fold of the N-domain of human eRF1 is the same in the crystal and solution structures but the detailed structures are far from identical [Fig. 1(A)]. The RMSD of the superposition of the heavy backbone atoms (C $\alpha$ , N, O, and C') of the family of 20 NMR structures onto the crystal structure of the N-domain is  $1.8 \pm 0.1$  Å.

To identify the goodness of fit of the solution and crystal structures and the regions of the maximum displacement, local RMSD values  $\rho_i$ <sup>27</sup> were calculated for local pairwise superposition of the two structures (Supporting Information Fig. S6). The thickness of the ribbon [shown in Fig. 1(C)] is pro-

portional to the  $\rho_i$  values, which reflects the degree of divergence of the local protein backbone geometry in the two structures.

**Minor protein conformer.** Signals from several amino acids of the N-domain of human eRF1 are observed in NMR spectra as double peaks, representing major (80–90%) and minor (10–20%) components. The assignment of the minor conformer peaks is based on the characteristic cross peaks in the 3D heteronuclear spectra, including the NOESY spectra. Supporting Information Fig S1 illustrates the two sets of signals in the <sup>15</sup>N–<sup>1</sup>H HSQC spectrum of the protein backbone and side chain amide groups.

## Discussion

A comparison of the structure of the N-domain in solution and in the crystal showed that its N- and C-termini and most of the protein loops show clear differences in their backbone conformations. This can either be due to real structural differences between the protein in the crystal and in solution or to the absence of the neighboring M- and C-domains in the structure solved by NMR. It is likely that the differences in the protein conformation of loop 115–

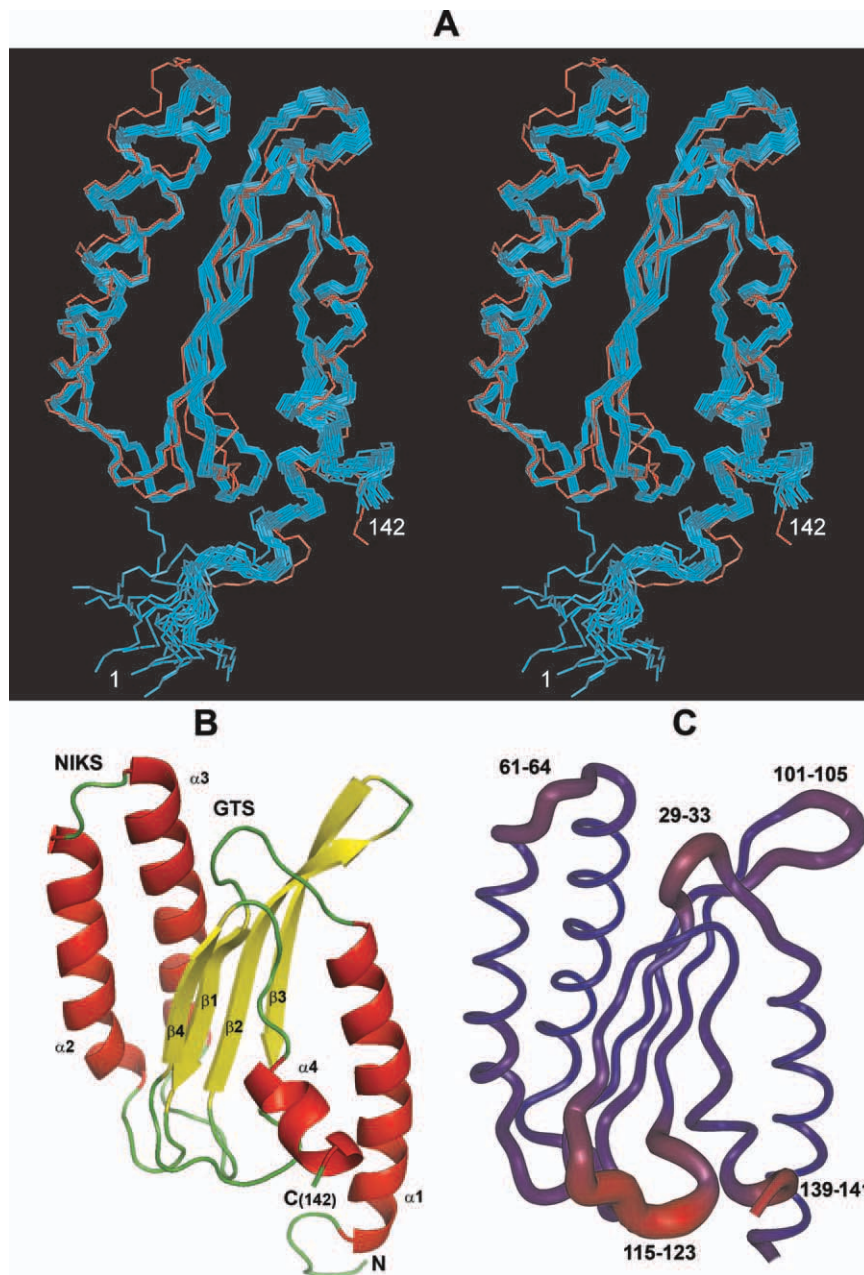


**Figure 1.** NMR solution structure of the N-domain of the human polypeptide chain release factor eRF1. (A). The stereo view of the ensemble of the final 20 calculated NMR structures superimposed on the heavy backbone atoms ( $C\alpha$ , N, and C) of the residues 6–142 of the representative structure. The crystal structure of the N-domain of the human eRF1<sup>8</sup> is superimposed on the same set of atoms and is shown in red. (B). The topology of the N-domain of human eRF1 and the secondary structure elements displayed using PyMol. (C). Ribbon representation of the backbone of the N-domain of human eRF1. The thickness of the ribbon is proportional to the RMSD values for the heavy atoms of each residue  $i$  after superposition of the family of 20 NMR structures onto the crystal structure using the set of backbone atoms of the four adjacent residues ( $i-2$ ,  $i-1$ ,  $i+1$ , and  $i+2$ ).

123 (having the largest RMSD values, Fig. 1(C), Supporting Information Fig S4B) and the C terminus originate from the absence of the neighboring M- and C-domains in the solution structure. The changes in residues 41–42 and 89–91 are likely to be secondary effects caused by the conformational change of loop 115–123. However, loops 29–33, 61–

64, and 101–105 [Fig. 1(C)] are all far from both M- and C-domains and therefore their large structural displacement is very likely to reflect real conformational differences between the crystal and solution states. It should be noted that loop 61–64 contains the conserved NIKS tetrapeptide sequence which is thought to be involved in the recognition of the



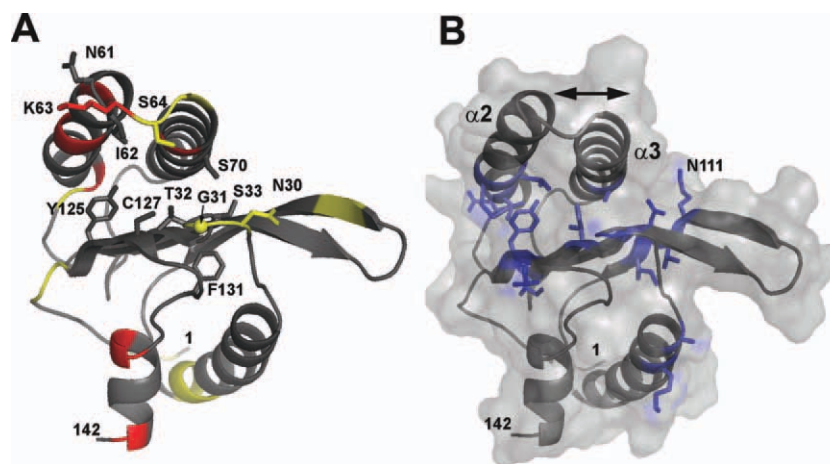


**Figure 2.** Dynamic and conformational behavior of the N-domain of human eRF1. (A). Representative structure of the N-domain colored in accordance with protein mobility on the ps–ns and ms time scale. Residues which have order parameters  $S^2$  less than 0.75 are colored yellow, and those which have substantial chemical exchange  $R_{ex}$  contributions to the transverse relaxation rate are colored red. The side chains of the functionally important residues are shown.  $C\alpha$  of residue G31 is also shown by a sphere. (B). A representative structure and molecular surface of the N-domain. Side chains of residues which have large chemical shift differences between the major and minor conformers are shown in blue. The arrow represents the hypothetical movement of the helices,  $\alpha 2$  and  $\alpha 3$ , which can explain special features of the two protein conformers.

first uridine of the stop codons<sup>20,21</sup> and the strictly conserved GTS loop sequence (position 31–33) which is implicated in the decoding of the stop codons.<sup>18,20,28,29</sup>

The ability of human eRF1 to recognize each of the three stop codons UAA, UAG, and UGA and to distinguish them from the UGG tryptophan codon cannot be explained in terms of a simple static interaction.<sup>30</sup> It is obvious that the N-domain of human eRF1 should be able to undergo conformational rearrangements – not only in solution but also inside the ribosome. Therefore the elucidation of the dynamic properties of this protein is crucial for understanding the mechanism of stop codon recognition. Model-free analysis of the relaxation data shows that there are several protein regions that undergo backbone motions with a correlation time of about 1 ns. Among these are residues 30–31, 64, and 122–123. Several other residues (45, 54–57, 63, 67, 134–135) were found to undergo conformational rearrangements on the ms time scale. These results are summarized in Figure 2(A), where residues undergoing fast (ns) motions are shown as yellow and those involved in slower (ms) motions are shown in red. It can be seen that two helices ( $\alpha 2$  and  $\alpha 3$ ), with NIKS loop between them, and two other loops (29–33 and 101–105) have high conformational plasticity. These protein regions are likely to be involved in stop codon recognition, either by their direct interaction with mRNA or by induced conformational rearrangements from the recognition sites.

Interesting information can also be obtained from an analysis of the residues which have duplicated signals in the NMR spectra and their distribu-

tion within the structure [Fig. 2(B)]. The duplication indicates that the protein exists in two conformational states with a ratio of the major to minor forms of about 5:1. Those residues which have large chemical shift differences between the two forms should be close to the center of the conformational rearrangement. Most of these residues are located at the interface between the  $\beta$ -sheet core of the protein and helices  $\alpha 2$  and  $\alpha 3$ . Their distribution [Fig. 2(B)] hints at a possible conformational rearrangement. This could be due to a change of helix orientation against the bundle of  $\beta$ -strands. For example, the chemical shifts of the side chain of Asn111 are substantially different between the major and minor protein conformations. It is very likely that residue Asn111, which is isolated in the major form, becomes close to the helix  $\alpha 3$  in the minor form.

It is of interest and possible mechanistic importance that the location of the highest amplitude internal motions, the residues from the GTS and NIKS loops of eRF1, coincide with the published experimental data suggesting that amino acids in these regions of the N-domain of eRF1 are essential for stop codon decoding.

## Materials and Methods

**Sample preparation.** The DNA fragment encoding the N-domain of human eRF1 (residues 1–142) with a C-terminal His<sub>6</sub>-tag fusion was cloned into the pET23b(+) vector (Novagen) under the phage T7 RNA polymerase promoter. N-eRF1 was overproduced in *E. coli*, strain BL21(DE3), in M9 minimal

medium and isolated using Ni-NTA resin (Qiagen). The protein was further purified by cation exchange chromatography using HiTrap SP columns (GE Healthcare). For  $^{13}\text{C}$ - and/or  $^{15}\text{N}$ -isotope labeling, [ $^{13}\text{C}_6$ ]-D-glucose and/or  $^{15}\text{NH}_4\text{Cl}$  (Cambridge Isotope Laboratories Inc.) were used as the isotope sources in M9 minimal medium. The samples for NMR (protein concentration  $\sim 1$  mM) were prepared in either 90%  $\text{H}_2\text{O}/10\%$   $\text{D}_2\text{O}$  or in 100%  $\text{D}_2\text{O}$  and 10 mM sodium phosphate, 25 mM NaCl, pH 6.8.  $\beta$ -mercaptoethanol ( $\sim 2$  mM) was added to the final solution to prevent oxidation of the free cysteine residues Cys97 and Cys127. Shigemi microcell NMR tubes, containing 330–380  $\mu\text{L}$ , were used for collection of the NMR spectra.

**NMR spectroscopy.** All spectra were acquired on Varian INOVA 600 and 800 MHz and Bruker AVANCE 600 MHz spectrometers equipped with triple resonance z-gradient probes. The 800 MHz spectrometer was equipped with a cryoprobe. Spectra were processed by NMRPipe<sup>31</sup> and analyzed using SPARKY.<sup>32</sup> Sequential backbone assignments and side chains assignments were obtained using the following 2D and 3D spectra: DQF-COSY, [ $^{13}\text{C}$ ,  $^1\text{H}$ ] HSQC, [ $^{15}\text{N}$ ,  $^1\text{H}$ ] HSQC, HNCB, HNCACB, CBCA (CO)NH, HBHA(CO)NH, HNHA, HNHB, HCC(CO)NH, and HCCH-TOCSY<sup>33</sup> measured at 298 K. Assignments were obtained for  $\sim 99\%$  of the  $^1\text{H}$ ,  $^{13}\text{C}$ , and  $^{15}\text{N}$  atoms of the protein backbone and for more than 90% of the side chains atoms. Backbone  $\phi$  and  $\psi$  dihedral angle restraints were determined from the chemical shift values of the backbone atoms  $^{13}\text{C}\alpha$ ,  $^{13}\text{C}\beta$ ,  $^{13}\text{C}'$ ,  $^1\text{H}\alpha$ ,  $^1\text{HN}$ , and  $^{15}\text{N}$  using TALOS+ software.<sup>34,35</sup> Side chain dihedral angles  $\chi_1$  were obtained by the AngleSearch program.<sup>36</sup> Residual dipolar coupling constants were measured using a partially oriented diluted liquid crystalline media composed of  $\sim 5\%$  v/w C12E5/hexanol.<sup>37</sup> The RDC values were calculated from the  $^1\text{D}_{\text{NH}}$  and  $^1\text{J}_{\text{NH}}$  constants, extracted from the IPAP-HSQC spectrum<sup>38</sup> acquired under anisotropic conditions, and the J-modulated HSQC experiment,<sup>39</sup> acquired under isotropic conditions, respectively.

**Structure calculation and refinement.** NOE distance restraints were determined from the [ $^1\text{H}$ ,  $^{13}\text{C}$ ] NOESY and [ $^1\text{H}$ ,  $^{15}\text{N}$ ] NOESY spectra measured at 298 K with a 100 ms mixing time. NOE peak volumes were calculated using the Sparky software.<sup>32</sup> The structure calculations and refinement were made by a simulated annealing protocol carried out in Cartesian coordinate space using CNS.<sup>40</sup> The restraint violations were monitored after each cycle of refinement by the NMRest program.<sup>24</sup> 2631 NOE-derived distance restraints, 316 dihedral angles, and 69 RDCs were used in the calculation of the final ensemble (see Supporting Information Table S1).

The structure quality has been analyzed with the AQUA and Procheck-NMR software<sup>41</sup> (Supporting Information Fig. S3). The best 20 structures out of 50 (with respect to the minimum restraints violation value criterion) were accepted as the final ensemble for each protein conformer. Structure visualization and analysis were carried out using the InsightII software package (Accelrys Software Inc.) and PyMol (DeLano Scientific LLC).

**NMR dynamics analysis.**  $R_1$ ,  $R_2$ , and  $^1\text{H}$ - $^{15}\text{N}$  heteronuclear NOE data sets of  $^{15}\text{N}$  uniformly labeled N-eRF1 were collected at 298 K on a 600 MHz Varian Inova spectrometer. The analysis of the  $R_1$ ,  $R_2$ , and  $^1\text{H}$ ,  $^{15}\text{N}$ -NOE values was carried out with a model-free formalism using the program RelaxFit written in-house.<sup>42</sup> All the details of the NMR relaxation data analysis are presented in Supporting Information.

**Databank accession numbers.** The  $^1\text{H}$ ,  $^{15}\text{N}$ , and  $^{13}\text{C}$  chemical shifts and the  $R_1$ ,  $R_2$ , and  $^{15}\text{N}\{^1\text{H}\}$  NOE values for protein backbone amides have been deposited in the BioMagResBank database (<http://www.bmrb.wisc.edu>) under the accession number BMRB-18092. The structural data and experimental restraints used in calculations have been submitted to the Protein Data Bank with the accession number 2LLX.

## Acknowledgments

The NMR measurements were carried out at the MRC Biomedical NMR Centre, Mill Hill, London, and Center for Magnetic Tomography and Spectroscopy, Moscow State University. This research is supported by the Medical Research Council, UK.

## References

1. Kisselev L, Ehrenberg M, Frolova L (2003) Termination of translation: interplay of mRNA, rRNAs and release factors? *EMBO J* 22:175–182.
2. Klaholz BP (2011) Molecular recognition and catalysis in translation termination complexes. *Trends Biochem Sci* 36:282–292.
3. Laurberg M, Asahara H, Korostelev A, Zhu J, Trakhanov S, Noller HF (2008) Structural basis for translation termination on the 70S ribosome. *Nature* 454:852–857.
4. Weixlbaumer A, Jin H, Neubauer C, Voorhees RM, Petry S, Kelley AC, Ramakrishnan V (2008) Insights into translational termination from the structure of RF2 bound to the ribosome. *Science* 322:953–956.
5. Korostelev A, Asahara H, Lancaster L, Laurberg M, Hirschi A, Zhu J, Trakhanov S, Scott WG, Noller HF (2008) Crystal structure of a translation termination complex formed with release factor RF2. *Proc Natl Acad Sci U S A* 105:19684–19689.
6. Ito K, Uno M, Nakamura Y (2000) A tripeptide ‘anticodon’ deciphers stop codons in messenger RNA. *Nature* 403:680–684.
7. Kisselev LL, Buckingham RH (2000) Translational termination comes of age. *Trends Biochem Sci* 25:561–566.

8. Song H, Mugnier P, Das AK, Webb HM, Evans DR, Tuite MF, Hemmings BA, Barford D (2000) The crystal structure of human eukaryotic release factor eRF1—mechanism of stop codon recognition and peptidyl-tRNA hydrolysis. *Cell* 100:311–321.
9. Cheng Z, Saito K, Pisarev AV, Wada M, Pisareva VP, Pestova TV, Gajda M, Round A, Kong C, Lim M, Nakamura Y, Svergun DI, Ito K, Song H (2009) Structural insights into eRF3 and stop codon recognition by eRF1. *Genes Dev* 23:1106–1118.
10. Frolova L, Seit-Nebi A, Kisselev L (2002) Highly conserved NIKS tetrapeptide is functionally essential in eukaryotic translation termination factor eRF1. *RNA* 8:129–136.
11. Inagaki Y, Doolittle WF (2001) Class I release factors in ciliates with variant genetic codes. *Nucleic Acids Res* 29:921–927.
12. Lozupone CA, Knight RD, Landweber LF (2001) The molecular basis of nuclear genetic code change in ciliates. *Curr Biol* 11:65–74.
13. Lekomtsev S, Kolosov P, Bidou L, Frolova L, Rousset JP, Kisselev L (2007) Different modes of stop codon restriction by the *Stylonychia* and *Paramecium* eRF1 translation termination factors. *Proc Natl Acad Sci U S A* 104:10824–10829.
14. Eliseev B, Kryuchkova P, Alkalaeva E, Frolova L (2011) A single amino acid change of translation termination factor eRF1 switches between bipotent and omnipotent stop-codon specificity. *Nucleic Acids Res* 39:599–608.
15. Salas-Marco J, Fan-Minogue H, Kallmeyer AK, Klobutcher LA, Farabaugh PJ, Bedwell DM (2006) Distinct paths to stop codon reassignment by the variant-code organisms *Tetrahymena* and *Euplotes*. *Mol Cell Biol* 26:438–447.
16. Ito K, Frolova L, Seit-Nebi A, Karamyshev A, Kisselev L, Nakamura Y (2002) Omnipotent decoding potential resides in eukaryotic translation termination factor eRF1 of variant-code organisms and is modulated by the interactions of amino acid sequences within domain 1. *Proc Natl Acad Sci U S A* 99:8494–8499.
17. Muramatsu T, Heckmann K, Kitanaka C, Kuchino Y (2001) Molecular mechanism of stop codon recognition by eRF1: a wobble hypothesis for peptide anticodons. *FEBS Lett* 488:105–109.
18. Bertram G, Bell HA, Ritchie DW, Fullerton G, Stansfield I (2000) Terminating eukaryote translation: domain 1 of release factor eRF1 functions in stop codon recognition. *RNA* 6:1236–1247.
19. Inagaki Y, Blouin C, Doolittle WF, Roger AJ (2002) Convergence and constraint in eukaryotic release factor 1 (eRF1) domain 1: the evolution of stop codon specificity. *Nucleic Acids Res* 30:532–544.
20. Bulygin KN, Khairulina YS, Kolosov PM, Ven'yaminova AG, Graifer DM, Vorobjev YN, Frolova LY, Kisselev LL, Karpova GG (2010) Three distinct peptides from the N domain of translation termination factor eRF1 surround stop codon in the ribosome. *RNA* 16:1902–1914.
21. Chavatte L, Seit-Nebi A, Dubovaya V, Favre A (2002) The invariant uridine of stop codons contacts the conserved NIKSR loop of human eRF1 in the ribosome. *EMBO J* 21:5302–5311.
22. Kolosov P, Frolova L, Seit-Nebi A, Dubovaya V, Kononenko A, Oparina N, Justesen J, Efimov A, Kisselev L (2005) Invariant amino acids essential for decoding function of polypeptide release factor eRF1. *Nucleic Acids Res* 33:6418–6425.
23. Seit-Nebi A, Frolova L, Kisselev L (2002) Conversion of omnipotent translation termination factor eRF1 into ciliate-like UGA-only unipotent eRF1. *EMBO Rep* 3:881–886.
24. Ivanova EV, Kolosov PM, Birdsall B, Kelly G, Pastore A, Kisselev LL, Polshakov VI (2007) Eukaryotic class 1 translation termination factor eRF1 – the NMR structure and dynamics of the middle domain involved in triggering ribosome-dependent peptidyl-tRNA hydrolysis. *FEBS J* 274:4223–4237.
25. Mantsyzov AB, Ivanova EV, Birdsall B, Alkalaeva EZ, Kryuchkova PN, Kelly G, Frolova LY, Polshakov VI (2010) NMR solution structure and function of the C-terminal domain of eukaryotic class 1 polypeptide chain release factor. *FEBS J* 277:2611–2627.
26. Oda Y, Muramatsu T, Yumoto F, Ito M, Tanokura M (2004) Backbone <sup>1</sup>H, <sup>13</sup>C and <sup>15</sup>N resonance assignment of the N-terminal domain of human eRF1. *J Biomol NMR* 30:109–110.
27. Polshakov VI, Morgan WD, Birdsall B, Feeney J (1999) Validation of a new restraint docking method for solution structure determinations of protein-ligand complexes. *J Biomol NMR* 14:115–122.
28. Bulygin KN, Khairulina YS, Kolosov PM, Ven'yaminova AG, Graifer DM, Vorobjev YN, Frolova LY, Karpova GG (2011) Adenine and guanine recognition of stop codon is mediated by different N domain conformations of translation termination factor eRF1. *Nucleic Acids Res* 39:7134–7146.
29. Wang Y, Chai B, Wang W, Liang A (2010) Functional characterization of polypeptide release factor 1b in the ciliate *Euplotes*. *Biosci Rep* 30:425–431.
30. Chavatte L, Frolova L, Laugaa P, Kisselev L, Favre A (2003) Stop codons and UGG promote efficient binding of the polypeptide release factor eRF1 to the ribosomal A site. *J Mol Biol* 331:745–758.
31. Delaglio F, Grzesiek S, Vuister GW, Zhu G, Pfeifer J, Bax A (1995) NMRPipe: a multidimensional spectral processing system based on UNIX pipes. *J Biomol NMR* 6:277–293.
32. Goddard TD, Kneller DG <http://www.cgl.ucsf.edu/home/sparky>.
33. Bax A, Grzesiek S (1993) Methodological advances in protein NMR. *Acc Chem Res* 26:131–138.
34. Cornilescu G, Delaglio F, Bax A (1999) Protein backbone angle restraints from searching a database for chemical shift and sequence homology. *J Biomol NMR* 13:289–302.
35. Shen Y, Delaglio F, Cornilescu G, Bax A (2009) TALOS plus : a hybrid method for predicting protein backbone torsion angles from NMR chemical shifts. *J Biomol NMR* 44:213–223.
36. Polshakov VI, Frenkiel TA, Birdsall B, Soteriou A, Feeney J (1995) Determination of stereospecific assignments, torsion-angle constraints, and rotamer populations in proteins using the program AngleSearch. *J Magn Reson B* 108:31–43.
37. Ruckert M, Otting G (2000) Alignment of biological macromolecules in novel nonionic liquid crystalline media for NMR experiments. *J Am Chem Soc* 122:7793–7797.
38. Ottiger M, Delaglio F, Bax A (1998) Measurement of J and dipolar couplings from simplified two-dimensional NMR spectra. *J Magn Reson* 131:373–378.
39. Tjandra N, Grzesiek S, Bax A (1996) Magnetic field dependence of nitrogen-proton J splittings in N-15-enriched human ubiquitin resulting from relaxation interference and residual dipolar coupling. *J Am Chem Soc* 118:6264–6272.

40. Brunger AT, Adams PD, Clore GM, DeLano WL, Gros P, Grosse-Kunstleve RW, Jiang JS, Kuszewski J, Nilges M, Pannu NS, Read RJ, Rice LM, Simonson T, Warren GL (1998) Crystallography & NMR system: a new software suite for macromolecular structure determination. *Acta Crystallogr D Biol Crystallogr* 54:905–921.
41. Laskowski RA, Rullmannn JA, MacArthur MW, Kaptein R, Thornton JM (1996) AQUA and PROCHECK-NMR: programs for checking the quality of protein structures solved by NMR. *J Biomol NMR* 8: 477–486.
42. Polshakov VI, Birdsall B, Frenkiel TA, Gargaro AR, Feeney J (1999) Structure and dynamics in solution of the complex of *Lactobacillus casei* dihydrofolate reductase with the new lipophilic antifolate drug trimetrexate. *Protein Sci* 8:467–481.